46th AIAA/ASME/ASCE/AHS/ASC Structures, Structural Dynamics & Materials Conference
18 - 21 April 2005, Austin, Texas

AIAA 2005-2048

Design & Manufacture of Stiffened Spring-Back Reflector Demonstrator

Lin Tze Tan*
Department of Civil & Environmental Engineering,
University College London,
Gower Street, London WC1E 6BT, UK
l.tan@ucl.ac.uk

Omer Soykasap† and Sergio Pellegrino‡
Department of Engineering,
University of Cambridge,
Trumpington Street, Cambridge CB2 1PZ, UK

Following many investigations into the Stiffened Spring-Back Reflector (SSBR) concept proposed by Tan & Pellegrino, a 0.8 m diameter demonstrator has been manufactured and tested. This paper details the design and manufacturing challenges encountered with this 0.8 m diameter triaxially woven Carbon Fiber Reinforced Plastic (CFRP) demonstrator. Although the SSBR concept was originally intended for deep parabolic dishes ($F/D = 0.28$), the requirements for the demonstrator are for a focal length to diameter ratio, F/D of 0.5 – a much flatter dish, hence redesign is required. Here we show the feasibility and effectiveness – analytically and experimentally – of applying the SSBR concept to a flatter dish, resulting in a 0.8 m diameter stiffened reflector with a fundamental frequency of 12 Hz, large initial resistance against packaging of about 117 N/m with good surface accuracy for a mass of less than 100 grams.

Introduction

The SSBR concept is based on a thin flexible carbon fiber reinforced plastic (CFRP) shell that is elastically folded as a single piece, without any joints or hinges, see Fig 1.

The folding concept is both simple and effective: opposite edges of the reflector are pulled towards each other by about half of their original distance and are held in place by tie cables – its largest stowed dimension being slightly larger than the deployed diameter. Once in orbit, the tie cables that hold the reflector in its packaged configuration are released and the reflector deploys dynamically by releasing its stored elastic strain energy. It should be noted that both Robinson[9] and Romeo *et al.*[10] have proposed similar packaging concepts involving the elastic folding of thin parabolic shells.

In order to be folded elastically, these reflectors need to have low stiffness, but it is precisely their low stiffness that makes it difficult for them to achieve and retain a high shape accuracy. Furthermore, the manufacturing process of thin CFRP structures leaves behind residual stresses that produce shape distortions in such highly flexible structures. These distortions are of the order of $D/1000$ in an unstiffened thin parabolic dish (D=4.6 m), and make it even more difficult to meet the stringent shape accuracy requirements imposed on communications antennas.

Hence the SSBR reflector is stiffened by attaching a collapsible rim around the edge of the dish. The stiffening rim significantly increases the overall stiffness of the dish in the deployed configuration and yet its configuration is such that the newly stiffened dish can still be folded elastically.

Experimentally verified results from an extensive finite element study of small scale models (D=0.45 m) have already been presented.[13] Results from an optimization procedure to consider the trade off between high deployed stiffness and ease of packaging for a large scale 4.6 m reflector concept have also been presented – these have shown great promise with excellent surface accuracy characteristics.[15]

In order to verify both the manufacturing process and the applicability of the triaxially woven CFRP material, a small scale 0.45 m diameter breadboard model has already been constructed and tested. This preliminary model was manufactured by a resin film infusion (RFI) process, the resulting physical model which was constructed from a single ply of triaxially

*Lecturer in Structural Mechanics
†Senior Research Associate
‡Professor of Structural Engineering

Copyright © 2004 by L.T.Tan. Published by the American Institute of Aeronautics and Astronautics, Inc. with permission.

Copyright © 2005 by L.T.Tan. Published by the American Institute of Aeronautics and Astronautics, Inc., with permission.

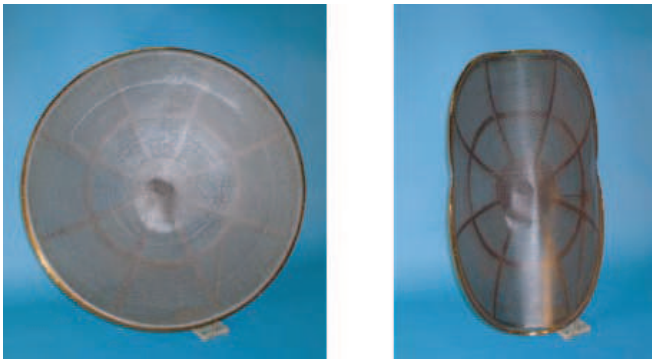

a) Plan View of SSBR demonstrator

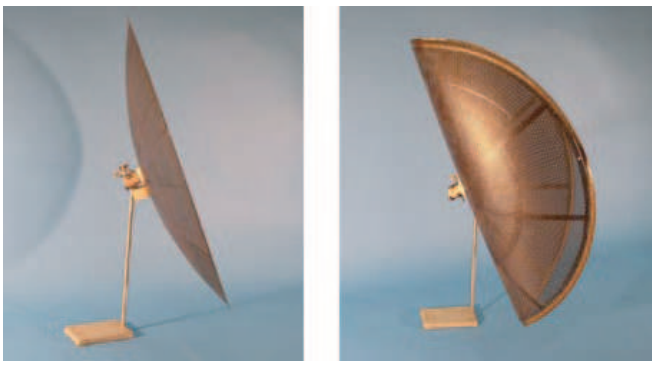

b) Side View of SSBR demonstrator

Fig. 1 Demonstrator in deployed and packaged configurations

woven CFRP has a mass of only 30 grammes.

The requirements for the demonstrator reflector are a plan diameter of 0.8 m and a focal length to diameter ratio $F/D = 0.5$. Previous studies by Tan & Pellegrino[13,15] on both small (0.45 m) and large (4.6 m) scale reflectors with $F/D \approx 0.28$ have considered the trade off between high deployed stiffness and high flexibility for packaging. Although these previous optimal designs can be used as starting points for the design of the 0.8 m demonstrator, the SSBR concept was originally intended for deep paraboloids $F/D \approx 0.28$. Flatter reflectors have less resistance to bending due to their shallowness and hence are less stiff. This extra flexibility calls for a redesign of the SSBR reflector concept. This paper details the required redesign of the SSBR stiffening system in order to be applied to the 0.8 m demonstrator together with its manufacturing process. Experimental results to both verify the finite element simulations and to ascertain the effectiveness of the concept will also be presented.

Stiffening Scheme

Stiffness dependency on F/D

In order to ascertain the effect of the F/D ratio i.e. dish shallowness, on deployed stiffness, it is useful to compare equal mass parabolas of different focal lengths. An analytical estimate of the fundamental natural frequency of a parabolic dish can be obtained by approximating the dish as a spherical cap of uniform thickness. This spherical equivalent to the parabolic reflector (Fig. 2) has a constant radius of,

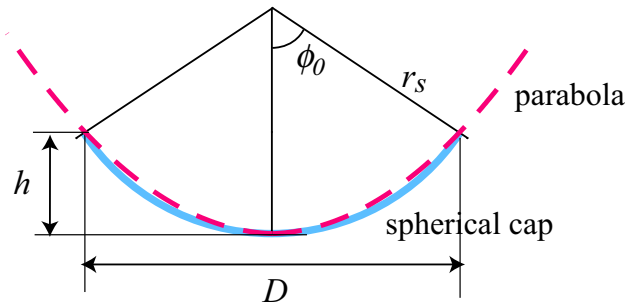

Fig. 2 Approximation of paraboloid with spherical cap.

$$r_s = 2F + \frac{D^2}{32F} \tag{1}$$

subtending an angle $2\phi_0$ where,

$$\phi_0 = \sin^{-1}\left(\frac{D}{4F + \frac{D^2}{16F}}\right) \tag{2}$$

The surface area of this spherical cap is

$$S = 2\pi r_s h = \pi((D/2)^2 + h^2) \tag{3}$$

where the height of the parabola $h = \frac{D^2}{16F}$

For a given material and thickness, the diameter of other equal mass paraboloids with focal lengths, F, can be obtained by solving equation for D,

$$D(F) = 4\sqrt{\frac{-2\pi F^2 - \sqrt{4\pi^2 F^4 + SF^2\pi}}{\pi}} \tag{4}$$

While the spherical equivalents to these equal mass paraboloids can be obtained using Equations (1) and (2)

The spherical equivalent to the parabolic 0.8 m diameter demonstrator with $F/D = 0.5$, has a spherical cap of radius $r_s = 0.85$ m, subtended angle $2\phi_0 \approx 56°$, height $h = 0.1$ m and hence a surface area of $S = 0.534$ m^2.

A good estimate of the fundamental natural frequency of these shell structures can be obtained[8] by assuming an inextensional mode of vibration of dimensionless amplitude A_i, with i (=2,3,...) circumferential waves. Considering a polar coordinate system r, θ, ϕ, the radial components of motion, denoted by the subscript r, have the expression

$$w_r = A_i r_s (i + \cos\phi) \tan^i \frac{\phi}{2} \sin i\theta \tag{5}$$

The corresponding hoop and meridional components are obtained by imposing the condition that no extension takes place.

Rayleigh[8] derived the following expressions for the strain energy, U, and kinetic energy, V, associated with harmonic vibration at angular frequency ω_i

$$U(i,\phi) = 2\pi(i^3-i)^2(1-\nu)\frac{Et^3}{12(1-\nu^2)}g_1(i,\phi)A_i^2\sin^2\omega_i t$$
$$V(i,\phi) = \frac{\pi}{2}\rho t r_s^4 g_2(i,\phi)\omega_i^2 A_i^2\cos^2\omega_i t$$

where

$$g_1(i,\phi) = \frac{1}{8}\left[\frac{\left(\tan\frac{\phi}{2}\right)^{2i-2}}{i-1}+\frac{2\left(\tan\frac{\phi}{2}\right)^{2i}}{i}+\frac{\left(\tan\frac{\phi}{2}\right)^{2i+2}}{i+1}\right]$$
$$g_2(i,\phi) = \int_0^{\phi}\left(\tan\frac{\phi}{2}\right)^{2i}\left[(i+\cos\phi)^2+2(\sin\phi)^2\right]\sin\phi\, d\phi$$

The form of the equations presented above is largely due to Blevins,[1] and the term $\frac{Et^3}{12(1-\nu^2)}$ represents the flexural stiffness of the shell.

The corresponding natural frequencies of vibration, obtained by equating the maximum strain energy (setting $\sin\omega_i t = 1$) to the maximum kinetic energy (setting $\cos\omega_i t = 1$) in each mode are then

$$f_i = \frac{\omega_i}{2\pi} = \frac{i^3-i}{2\pi}\sqrt{\frac{E/\rho}{3(1+\nu)}}\sqrt{\frac{g_1}{g_2}}\frac{t}{r_s^2} \quad \text{for } i = 2,3,4.....$$

where f_i is the natural frequency of mode $(i-1)$.

This equation shows that for any value of i the frequency of a spherical cap is inversely proportional to the square of its radius and to the factors g_1 and g_2, which are dependent on the focal length, F through the subtended angle, ϕ. The dependence on the F/D ratios of the original paraboloids is hidden behind these different factors and is more readily capture by plotting the first fundamental frequency, f_2 against F/D. This relationship is illustrated in Fig. 3 and is dominated by a D^2/F^2 term.

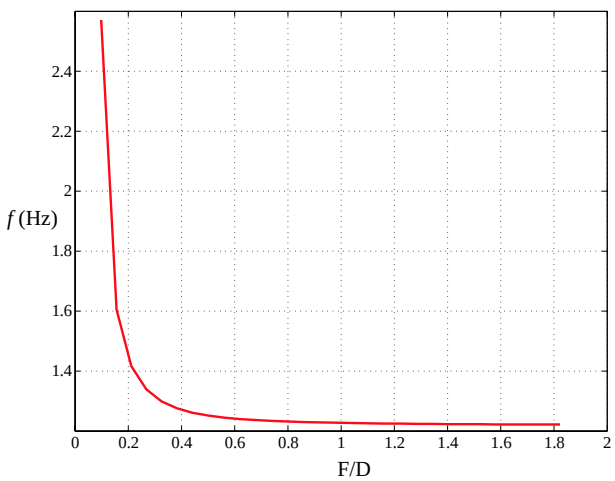

Fig. 3 Variation of fundamental natural frequency with F/D ratio for equal mass paraboloids

For a homogeneous triaxially woven CFRP shell with thickness, $t = 0.13$ mm,the fundamental deployed frequency of the $F/D = 0.5$ demonstrator is 1.25 Hz. While a deeper equal mass paraboloid with $F/D = 0.28$ (equivalent spherical cap radius $r_s = 0.76$ m and $2\phi \approx 92°$) has a frequency of 1.32 Hz, a difference of about 6%.

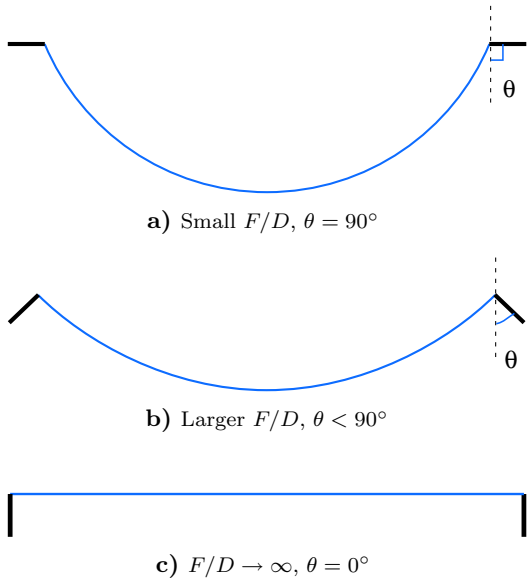

Fig. 4 Variation of stiffener angle, θ (measured from the vertical) with F/D ratio. Stiffeners shown in bold

Tuneable Stiffener

Hence it can be seen that for a given mass, flatter shells with $F/D > 0.4$ have low stiffness. The extreme case is of course a shell with $F/D \to \infty$ or rather a flat plate. In order to stiffen this, one would increase the plate's bending stiffness which is directly related to its second moment of area I. Increasing the plate thickness would increase I, however this is not efficient in terms of mass. The addition of perpendicular flanges, Fig 4(c) is instead a much more effective method of increasing the flexural stiffness of the plate. This method of preventing the structure from deforming in its lowest stiffness eigenmode is the type of reasoning behind the stiffening system of the SSBR. Previous investigations[12] for deep dishes ($F/D = 0.28$) have shown a stiffener angle, $\theta = 90°$ (Fig 4(a)) to be the best trade-off between deployed stiffness and folding flexibility. However as the F/D ratio increases more stiffness is needed and hence the stiffener angle (Fig 4(b)) tends towards that of the flat plate. Alternatively the actual geometry of the stiffener could be altered.

The problem with a continuous stiffening skirt or ring, is that it makes the reflector so stiff that it can no longer be folded elastically. This is not surprising as, in general, the stiffer one makes a structure, the "harder" it becomes to deform it elastically. If the force displacement relationship is linear, the strain en-

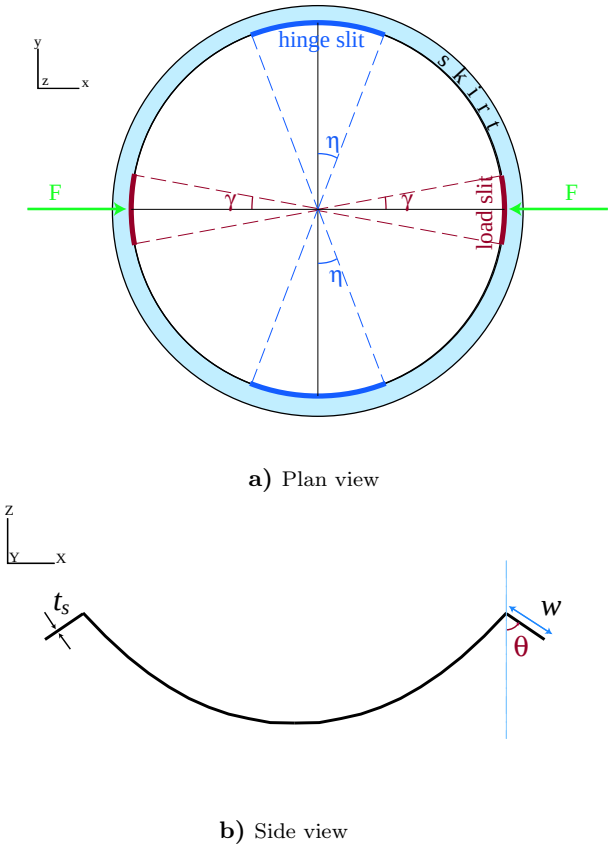

a) Plan view

b) Side view

Fig. 5 Adjustable parameters of the stiffening system

ergy in the structure - equal to the work done by the forces that impose the deformation - is proportional to the "stiffness" of the structure. Thus, the strain energy required to deform a stiffer structure by the same amount will be proportionally greater. The maximum strain and stress in the structure will also increase proportionally.

This problem has been addressed by introducing a small number of circumferential slits between the stiffener and the rim of the dish (Fig 5) resulting in a system whose stiffness can be tuned as required. A potentially negative effect of introducing cuts in any structure, is of course, that they can result in high stress concentrations. However, these can be eliminated by controlling the stiffness distribution near the cuts and by designing out sharp edges, details of this can be found in an earlier paper.[15] A particular feature that is obtained in some cases is that the slits allow sections of the stiffener to 'snap' through while the reflector is being folded, hence decreasing the force required to fold the reflector. This is due to the fact that these slits enable the formation of a series of localised buckles, each spanning the width of the slit.

Hinge slit angles (Fig 5(a)) are crucial in allowing large portions of the dish to bend when the reflector is being packaged – therefore reducing peak strains in the dish. Hence in general, these slits dictate the

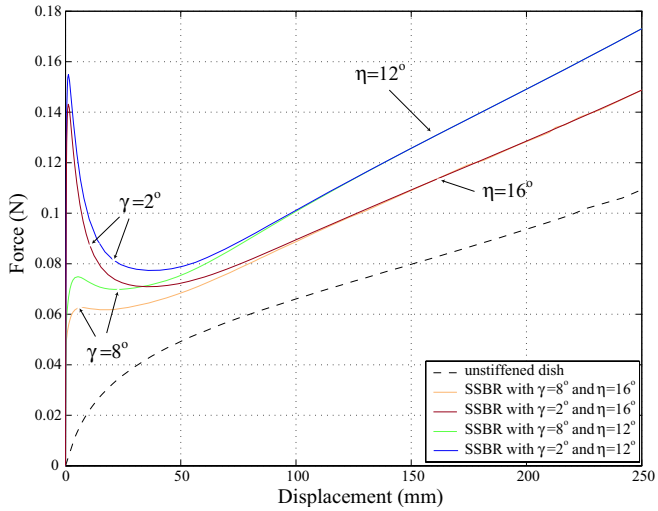

Fig. 6 Effect of increasing slit angles

peak stress in the dish and the final packaged force of the reflector. Fig 6 illustrates the force-displacement behaviour of the packaging process. From this, it is apparent that increasing the hinge slit angle, η reduces the packaging forces.

On the other hand, load slits allow the stiffener/skirt to buckle elastically during packaging and hence in general, control the peak snapping/buckling load. Fig 6 shows that decreasing the load slit angle, γ will increase the peak snapping force. Conventionally, buckling is a phenomenon which engineers design against. However, in the present context we exploit the fact that once a part of a structure buckles, the overall system looses some of its load-carrying ability and stiffness. This is the very basis of our stiffness-tuning method.

Other variable parameters of the SSBR are the stiffener/skirt width (larger widths giving higher stiffnesses), the stiffener angle and thickness.

Demonstrator Configuration

Reinforcement Schemes

The surface of the demonstrator is constructed from a single ply of triaxially woven CFRP ($t = 0.13$ mm). In order to prevent local deformations of this ultra thin surface, reinforcements were introduced, Fig 7. The placement of reinforcing radial ribs was considered first (Configs I-II), and subsequently the ribs in the configuration with the most promise were connected to form smaller segments (Configs III-VIII). The reinforcement patterns were kept simple for ease of manufacturing. Configs III and IV have triangulated segments whereas in Configs V-VIII the 8 large sectors of the dish were subdivided by a circular ring of reinforcement about 0.6R from the center. To prevent distortions under gravity and to provide a stiff attachment point, the hub of diameter 200 mm was also reinforced.

The rim of Configs I-V, VII was strengthened by an edge reinforcing ring running tangentially along the

surface. This was added for extra stiffness and to terminate the ultra thin surface of the dish. Due to an error during manufacture, the reinforcement pattern of Config VIII represents the setup that was constructed – the edge reinforcing ring is absent from this configuration.

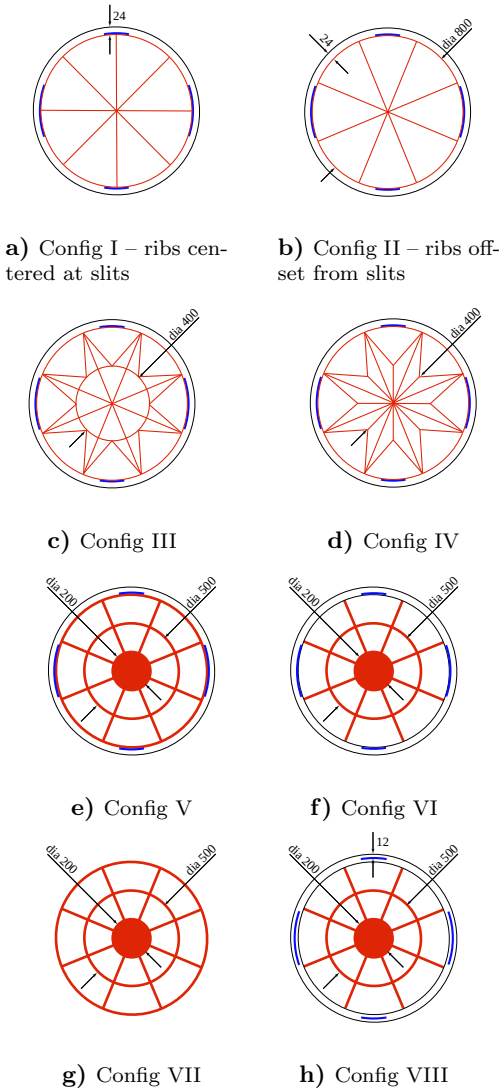

a) Config I – ribs centered at slits **b)** Config II – ribs offset from slits

c) Config III **d)** Config IV

e) Config V **f)** Config VI

g) Config VII **h)** Config VIII

Fig. 7 Different reinforced configurations (all dimensions in mm). Reinforcements shown in red and slits in blue

All reinforcements were created by laying up an extra ply of material on the non-reflecting surface of the dish, hence the total thickness of the reinforcements is 2 plies or 0.26 mm. The reinforcements in Configs I-IV are 10 mm wide while for ease of manufacturing, Configs V-VIII have 20 mm wide reinforcements.

Stiffener Configuration

Depending on the design criterion, optimal configurations of 0.45 m and 4.6 m diameter SSBRs have stiffener angles of about 90° (both reflectors had similar F/D ratios), stiffener widths between 3%-10% of the radius, load slit angles, γ varying between 0.5°-8° and hinge slit angles, η from 7°-18° (see Fig 5 for clarification).[14] The large variation is due to the chosen limit on the maximum stress in the reflector – if the limit stress is difficult to achieve optimal designs tend to have larger slit angles and narrower stiffener widths. Using these optimized ranges, a starting point for the 0.8 m demonstrator design was chosen to have a stiffener width of $0.06R = 24$ mm, load angle $\gamma = 7°$, hinge angle $\eta = 14°$ and a stiffener thickness of 2 material plies. Initial comparisons of the reinforcement schemes were performed with a stiffener angle, $\theta = 90°$.

However configurations with flat stiffeners tend to suffer from the localized buckling of the unsupported lengths of the stiffener adjacent to the slits.[3] Hence in order to increase the bending stiffness of the reflector and to prevent this localised buckling, a curved stiffener was introduced, Config VIII. Note that Config VIII has the same reinforcement pattern as Config VI but a curved stiffener instead of a flat horizontal one, and is also of an equal mass. Hence the curved stiffener is a circular arc of $r = 20$ mm subtending an angle of 69°. This results in a plan stiffener width of 22.6 mm, compared to that of 24 mm in Config VI. It also worth noting that Config VIII has slits in the middle of the stiffener rather than at the connection between the stiffener and the rim of the dish.

Config VII has the same reinforcement pattern as Config V, but no stiffener and is used as a reference configuration.

Computational Details

The particular structure that has been analysed forms an axisymmetric paraboloid of equation

$$z = \frac{x^2 + y^2}{4F} \tag{6}$$

where F is the focal length. The focus to diameter ratio is $F/D = 0.5$, the diameter of the aperture is $D = 800$ mm and hence, the height of the rim is $h = 100$ mm. The geometry and the finite element mesh were created in the ABAQUS CAE,[6] see Fig 8. To keep computational times low, half of the dish was analysed, using the appropriate symmetry boundary conditions.

The surface of the reflector and all reinforcements i.e. ribs, triangulations and edge ring were modelled as linear 3-noded triangular shell elements (S3R). Consistent convergence was achieved with a fine mesh of these general purpose elements (density of 8600 elements per half dish) and 4 noded quadrilateral elements (S4R) for the stiffener(1800 elements) – together with the default ABAQUS iteration control parameters. S3R and S4R elements are general purpose shell elements which account for finite membrane strains and will allow for changes in thickness and are therefore, suitable for large-strain analysis. These elements

use reduced (lower-order) integration, which significantly reduces run times in three dimensions.[6] According to the ABAQUS manual, these elements provide accurate results, provided that they are not significantly distorted and/or loaded in in-plane bending.[6]

The slits between the dish and the stiffener were modelled as voids and hence have a finite width of 3 mm.

All simulations were performed with ABAQUS running on a Pentium IV 2.2 GHz PC; the average run time for the non curved stiffeners was 10 minutes, while Config VIII ran for 40 minutes. A typical analysis consisted of two steps, the first being a linear eigenvalue analysis, to extract the natural frequencies and eigenmodes of the reflector in its deployed configuration, and the second step being a geometrically non-linear simulation of the folding of the reflector.

The first step is an eigenvalue extraction using the *FREQUENCY command with the default 'subspace' eigensolver in ABAQUS. The first 20 eigenmodes were extracted and the maximum frequency of interest was set to 40 Hz. The fundamental natural frequency which is used as a measure of the reflector's stiffness in the deployed configuration is obtained from this step.

The second step is a geometrically non-linear static analysis that simulates the folding of the reflector under displacement control. This uses the *STEP, NLGEOM and *STATIC options in ABAQUS. Moving boundary conditions were applied to the rim of the reflector, to impose a total displacement of about $D/3$.

The initial slope of the force-displacement relationship, k, which represents the resistance to folding, the maximum stress, σ_{max}, the maximum force that needs to be applied to fold the reflector, F_{peak}, and the final value of the force required to hold the reflector in its packaged configuration, F_{final}, were all extracted from this final step.

A further sperate buckling analysis of the full demonstrator model which is fixed in the center was performed in order to determine the components of the reflector which are most prone to buckling. The static buckling analysis option in ABAQUS was used to subject the demonstrator to unit (translational) acceleration loads (using the *gravity option) that are applied quasi-statically and independently of one another, in the x, y, and z directions.

Material & Manufacturing Details

Triaxially woven CFRP

SK-802 fabric from Sakase-Adtech Ltd., Japan was used in the construction of both the small scale 0.45 m model and the 0.8 m demonstrator. This fabric is woven from Toray T-300 yarns at orientations of +60, 0, -60. The yarns are woven into the basic weave pattern which results in hexagonal open hole sections (Fig 9(a))with a low fiber volume fraction and hence mass per unit area– dimensions of a unit cell of SK-802 are given in Fig 9(b). CFRP made from this type of triaxially woven fabric has a nearly isotropic elastic modulus[5,11,17] and high in-plane shear rigidity. Furthermore triaxial woven fabrics have much better mechanical behaviour (no obviously weak direction) compared to biaxially woven fabrics of the equivalent thickness.

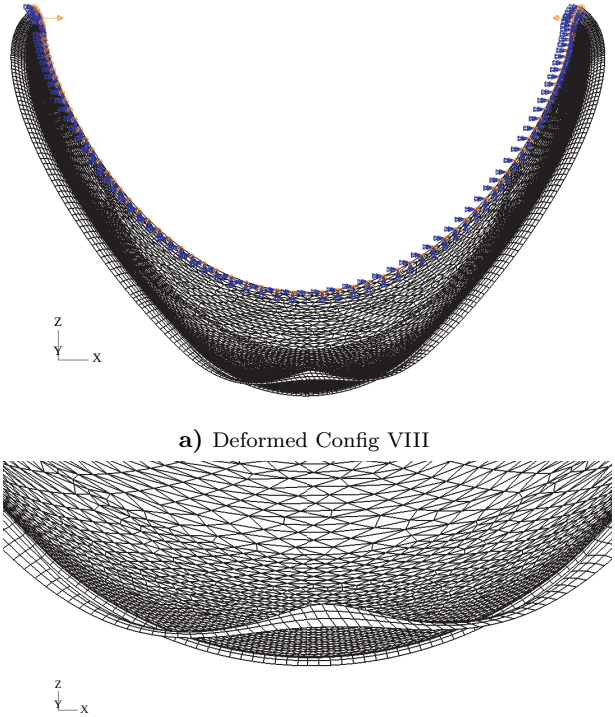

a) Deformed Config VIII

b) Detail of hinge slit

Fig. 8

The matrix of the composite is modified epoxy[2] HexPly 913 from Hexcel Composites, UK, which has a low temperature cure cycle (125°C).

The final composite, SK-802/913 has a thickness of 0.13 mm, a measured density of 920 kg/m^3, Young's modulus of 29.4 GPa and a tensile strength of 250 MPa, and a maximum strain in bending of 2.3% (measured by Yee *et. al*[18]).

The coefficient of thermal expansion (CTE) of SK-802/913 in the 0° and 90° directions was experimentally measured[3] to be 2.35×10^{-6} and 1.61×10^{-6}. Matsumoto[7] has also shown that triaxially woven CFRP composites have on the whole, good RF characteristics for reflectors operating up to Ka-band (30 GHz), with near zero CTE.

The material properties of the carbon fiber, triaxial fabric, epoxy and final composite are listed in Table 1.

Manufacture

Due to the size of the demonstrator, the mould had to be manufactured in three separate parts along the height of the dish. The three separate parts which were

Property	T-300 carbon fiber	SK-802 fabric	Hexcel 913 epoxy	SK-802/913 composite
Thickness (mm)	-	0.14	-	0.13
Density (kg/m^3)	1750	75 (g/m^2)^a	1230	920
Elastic Modulus (GPa)	235	-	3.4	29.4
Tensile Strength (MPa)	3820	-	65.5	250
Maximum strain (%)	1.6	-	-	2.4^b

^{a}areal density
^{b}maximum surface strain in bending[18]

Table 1 Material Properties of T-300 Carbon fibers, SK-802 triaxially woven dry fabric, H913 epoxy and SK-802/913 triaxially woven CFRP. The material properties for SK-802/913 are measured ones.

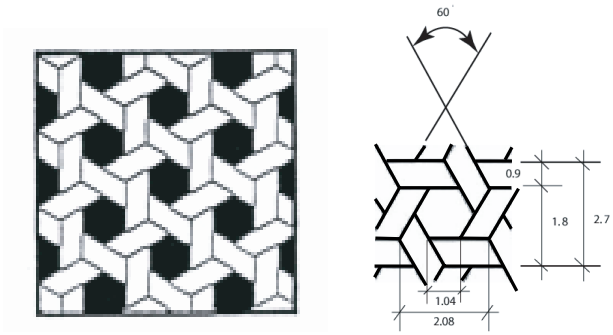

a) Basic weave pattern with hexagonal open hole sections **b)** Dimensions of a unit cell of SK-802 in mm

Fig. 9 Triaxially woven SK-802 fabric

constructed from modelling board were then glued together using an epoxy adhesive to form a male mould.

The demonstrator was manufactured using the resin film infusion (RFI) process in which the dry triaxial fabric was laid up in between sheets of the semi-solid resin film supplied on release paper. The lay-up is then heated and pressure applied to allow the resin to first melt and then flow into the fabric. The HexPly 913 is tacky or slightly adhesive at room temperature (with a tack life of 30 days at 23°C), and hence the prepreg is kept refrigerated to about -10°C until required. Before curing, the prepreg sheets were cut to form 8 sectors and laid up on the mould to form the reflecting surface. The reinforcements were then laid up as extra layers on the non reflecting side. The structure was then cured in an autoclave at 125°C and at a pressure of 7 bar for 60 minutes – with a heat rate between 2°C-8°C.

Experiments

Surface Accuracy

The surface of the physical model was measured using photogrammetry. Ninety eight coded targets were attached to the surface of the model which was suspended vertically. In order to prevent rotation of the reflector, the center of the dish was lightly attached to the backing board. The reflector was then photographed from 9 different stations at different angles. The photogrammetry software PhotoModeler Pro[4] was used to identify the coded targets and calculate their coordinates. An optimization routine with 7 parameters, e.g. the focal length of the reflector F, 3 translations (x_0, y_0, z_0) and 3 rotations expressed as Euler angles (ϕ, θ, ψ) was used to find the best fit paraboloid. The variations between this best fit paraboloid and the target points were then tabulated and the root mean square (RMS) surface accuracy determined.

PhotoModeler gives 3D coordinates of the target points based on a user coordinate system xyz, in which axes are chosen to be approximately close to XYZ coordinate system of the best fit paraboloid. Conversion from xyz coordinate system to XYZ coordinate system can be written as follows:

$$\begin{bmatrix} X \\ Y \\ Z \end{bmatrix} = \mathbf{BCD} \begin{bmatrix} x \\ y \\ z \end{bmatrix} + \begin{bmatrix} x_0 \\ y_0 \\ z_0 \end{bmatrix} \tag{7}$$

where $\mathbf{B}$, $\mathbf{C}$, $\mathbf{D}$ are rotation matrices defined as

$$\mathbf{B} = \begin{bmatrix} cos(\psi) & sin(\psi) & 0 \\ -sin(\psi) & cos(\psi) & 0 \\ 0 & 0 & 1 \end{bmatrix}$$

$$\mathbf{C} = \begin{bmatrix} 1 & 0 & 0 \\ 0 & cos(\theta) & sin(\theta) \\ 0 & -sin(\theta) & cos(\theta) \end{bmatrix}$$

$$\mathbf{D} = \begin{bmatrix} cos(\phi) & sin(\phi) & 0 \\ -sin(\phi) & cos(\phi) & 0 \\ 0 & 0 & 1 \end{bmatrix}$$

For n target points that are equally spaced on the surface, RMS error in the axial direction Z, with respect to the best fit parabola, is calculated as

$$\delta_{ez} = \sqrt{\frac{\sum(\hat{Z}_i - Z_i)^2}{n}} \tag{8}$$

where $\hat{Z}_i$ is the axial coordinate of a general target point and Z_i is the corresponding axial coordinate of the best fit parabola.

Packaging

Displacement controlled static packaging tests were carried out vertically in an INSTRON testing machine

with specially machined fittings; the set up is shown in Fig 10. The connection between the rim of the dish and the INSTRON is through a 2 mm diameter ball and socket joint, which ensures that the edge of the dish is free to rotate through a large angle during folding; a detailed view is shown in Fig 10(c). The folding experiments were terminated after 200 mm displacement as the gravity loading on the dish localised the folding along a region aligned with the end of the hinge slits (Fig 10 (b)) instead of in the middle of the unstiffened area of the dish adjacent to the hinge slits. This localization does not occur when the reflector is packaged in the horizontal plane.

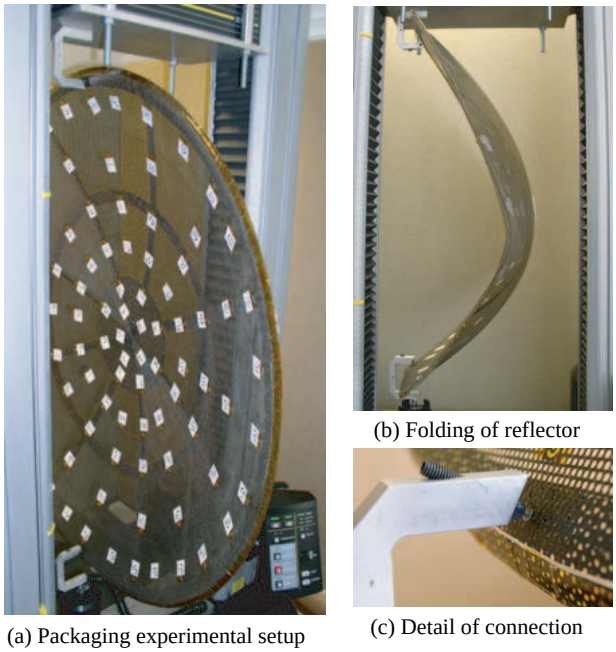

(a) Packaging experimental setup

(b) Folding of reflector

(c) Detail of connection

Fig. 10 Experimental setup for packaging characterization

Results and Discussion

The results in Table 2 reveal Config II – with ribs offset from the slits – to be the better radial rib placement strategy. For the same mass, Config II has a higher deployed fundamental frequency and lower packaged stress than Config I.

It can be observed from Table 2 that the added mass of the extra reinforcements in Configs III-VI actually decreases the frequency of these deployed reflectors. Hence the configurations with only radial ribs actually perform better, however the extra reinforcements are required to prevent local buckling on the ultra thin surface of the dish. To avoid this effect, the width of the triangulations could be reduced but due to manufacturing concerns, this was not realized and in reality the manufactured design has 20 mm wide reinforcements for ease of manufacture. This extra mass effect of lowering the deployed frequency is also evident when comparing Config V and Config VI – here the only difference is the rim reinforcement, which accounts for less than 7% of the total mass– the removal of the rim reinforcement increases the deployed frequency by about 1%.

The force displacement characteristics of all the configurations with flat horizontal stiffeners Configs I-VII are plotted in Fig 11. A characteristic common to these configurations is that they show a snapping behaviour after an initially linear response. This is also evident from Column 7 in Table 2 as ratios of $F_{final}/F_{peak} < 1$ indicate 'snapping'. This type of behaviour is very desirable as the structure *locks into the fully-deployed configuration* and yet it *folds rather easily, after some initial resistance.* Considering the fact that all these stiffened configurations have identical slit and stiffener widths – parameters which have been shown to dominate the packaging behaviour[16]– it is not surprising that the force displacement behaviours are all relatively similar. Comparison with a configuration without stiffener, Config VII, demonstrates the significant amount of added stiffness provided by the stiffeners.

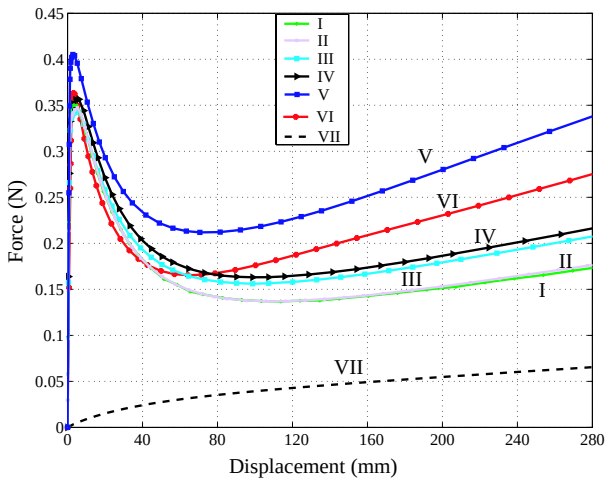

Fig. 11 Packaging behaviour of different reinforcement schemes

Although, Config III and IV with the triangulated reinforcement patterns have slightly lower masses and higher frequencies, Configs V and VI have lower peak stresses and are easier to manufacture and hence these configurations were selected.

Besides preventing the local buckling of the stiffener, the curved stiffener was introduced to increase the rather low peak packaging forces (Table 2). The effect of the curved stiffener Config VIII is evident from Fig 12(a), the initial stiffness, k has increased by nearly 17% but more importantly, the peak packaging force, F_{peak} has increased by a factor of 2.7 when compared to Config VI. The low deployed frequency of Config VIII is due to the plan stiffener width which is only 11 mm – half that of the other configurations. Although the peak stress is significantly higher for the

Config	f Hz	σ_{max} (N/mm^2)	k/k_{ref}	F_{peak} (N)	F_{final} (N)	F_{final}/F_{peak}	mass (gram)	stiffener details
I	20.34	78.7	333	0.35	0.18	0.51	84	24 mm
II	20.35	78.1	326	0.35	0.18	0.53	84	24 mm
III	19.82	82.9	243	0.34	0.21	0.62	89	24 mm
IV	19.90	81.7	252	0.36	0.22	0.63	90	24 mm
V	18.54	73.9	299	0.41	0.35	0.87	96	24 mm
VI	18.71	61.8	185	0.36	0.29	0.79	90	24 mm
VII	1.66	66.8	1	0.07	0.07	1.00	82	-
VIII	11.91	130.8	216	0.98	0.79	0.81	90	12 mm curved

Table 2 Finite Element simulation results. $k_{ref} = 0.54$ **N/m**

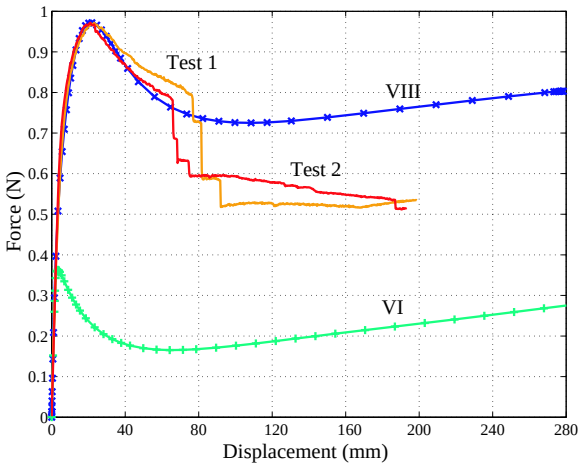

a) Full behaviour

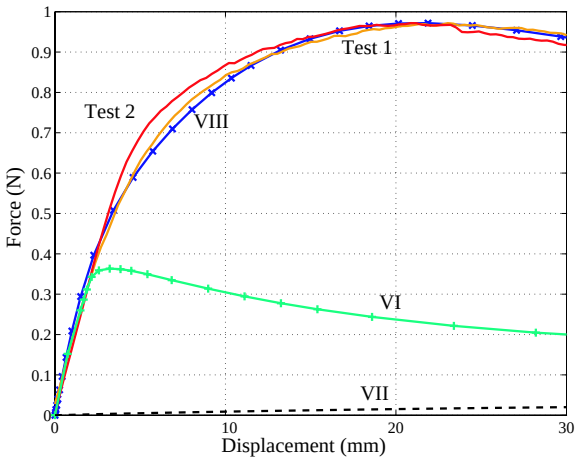

b) Initial stiffness

Fig. 12 Packaging behaviour of experimental and finite element simulations

curved stiffener configuration, there is still a safety factor of nearly 2 on the breaking stress of the composite.

In order to establish that the unsupported lengths of the curved stiffener are no longer prone to localized buckling, a static buckling analysis was conducted on a reflector with a Config V reinforcement pattern but a curved stiffener. The lowest buckling load of the demonstrator corresponds to an acceleration of 380 m/s^2 in the y-direction, this first mode manifests itself as a global rotation about x-axis as seen in Fig 13. Furthermore there was no significant mode which corresponded to the localized buckling of the stiffener.

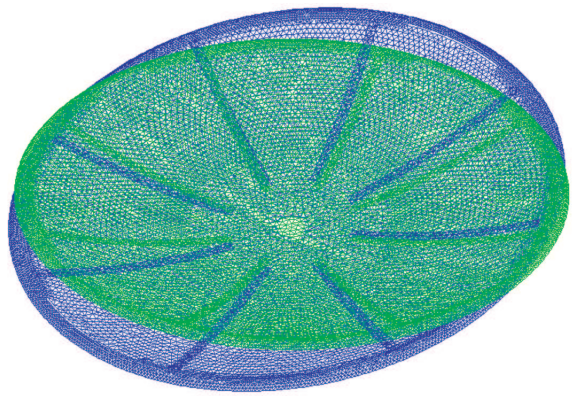

Fig. 13 First buckling mode of demonstrator model – rotation about x-axis

Experimental Results

Surface Accuracy

Using an optimization routine to minimize the error between the coordinates of the measured target points and a parabola with 7 adjustable parameters, the best fit parabola to the measured target points has a focal length of 0.395 m. Note that the mould was manufactured to have a focal length of 0.4 m, this 1.25% difference may be due to this highly flexible reflector's distortions under gravity. The rms surface error for this demonstrator was calculated to be 0.789 mm. This rather disappointing value is due to errors during manufacture. At the cure temperature, the epoxy adhesive used to fasten the 3 separate parts of the mould melted and hence a permanent meridional deformation of nearly 1 mm occurred in the surface of the reflector where the adhesive flowed out from the mould. The mould has been repaired and covered with a high temperature coating to prevent this defect from occurring in future models and hence the rms error for future models is expected to be much better.

Packaging Tests

The force displacement packaging behaviour of the demonstrator model is plotted in Fig 12(a) and (b). Note that the displacement is for one loaded point only, and the total distance the reflector is packaged is twice this. As mentioned earlier, the experiments were terminated after 200 mm of total displacement as the gravity loading on this ultra lightweight reflector concentrated the deformation in a narrow region aligned with the lower tip of the hinge slits (Fig 14) This behaviour was only observed in vertical packaging tests.

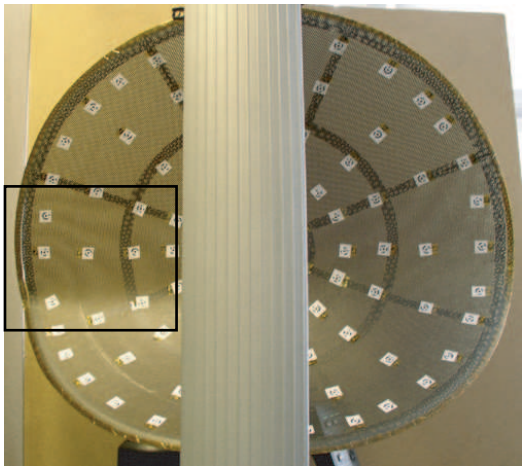

a) Packaging of demonstrator

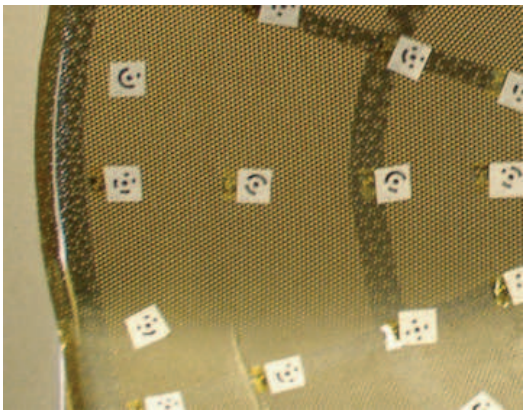

b) Detail of deformation localization at edge of slit

Fig. 14 Localization of deformation in the vertical packaging test

The finite element simulation results for Config VIII – corresponding to the physical demonstrator– is also plotted in Fig 12. There is good correlation between the experimental and FE results for displacements up till 60 mm with excellent agrement in the initial stiffness regime Fig 12(b). At the start of packaging until a displacement of about 60 mm the unsupported stiffener adjacent to the hinge slit, twists up and out away from the the surface of the reflector similar to the FE model, see Fig 8. However the stiffener is very narrow – this portion behaves like a column under compression and hence after a certain amount of compression i.e. 60 mm of displacement, the stiffener buckles back towards the surface of the dish, (Fig 14(b)). The unsupported portion of the stiffener losses the majority of its load carrying capacity and hence the packaging force reduces suddenly. Once one of the unsupported lengths of the stiffener has buckled, the other side follows quickly and hence this causes the stepped behaviour in the force displacement plot. In the large displacement regime the FE simulations and the experiments do not agree as the instabilities of the stiffener are not very easily modelled.

Conclusions

Triaxially woven CFRP SK-802/913 has been shown to have suitable properties for use in the construction of reflector antennas. It has been established that the SSBR concept is applicable to flatter reflectors – configurations considered have substantial stiffness increases without compromising the ability to fold the reflectors elastically. Curved stiffeners prevent the localised buckling of the unsupported lengths of the stiffener and significantly increase the peak packaging forces required to fold the reflector and hence increase its flexural stiffness. Packaging experiments have been used to verify the FE models, good agreement between FE and experimental results was obtained for the initial stiffness regime but the instabilities involved in the buckling of the stiffener in the physical model proved difficult to model in the FE simulations and will be further investigated.

The resulting 0.8 m diameter stiffened reflector has a fundamental frequency of 12 Hz, considerable increase in initial resistance against packaging, a factor of 216 compared to an unstiffened reflector, with reasonable surface accuracy of 0.78 mm, a peak packaging force of about 1 N and is extremely light weight – a mass of less than 100 grams.

References

[1]Blevins, R. D. *Formulas for Natural Frequency and Mode Shapes.* Krieger Publishing Company, ch. 12, pp. 330–334.

[2]Composites, H. Hexply 913. Product Datasheet, Duxford, Cambridge, UK. Publication FTA054b (Oct 2002).

[3]Datashvili, L., Lang, M., Zauner, C., Baier, H., Soykasap, O., Tan, L. T., Kueh, A., and Pellegrino, S. Technical assesment of high accuracy large space borne reflector antenna (tahara). Technical Report ESA Contract number 16757/02/NL/LvH/bj, Technical University of Munich, 2005. Ref.: LLB-R-12/07/04-02D-02.

[4]Eos Systems Inc. *PhotoModeler Pro*, 5.2 ed. ancouver BC Canada V6J 1Y6.

[5]Fujita, A., Hamada, H., and Maekawa, Z. Tensile properties of carbon fiber triaxial woven fabric composites. *Journal of Composite Materials 27*, 15 (1993), 1428–1442.

[6]Hibbitt, Karlsson, and Sorenson. *ABAQUS Standard Users Manual Version 6.1.* Hibbitt, Karlsson and Sorenson, Hibbitt, Karlsson & Sorenson, 1080 Main Street Pawtucket, Rhode Island 02860-4847 , USA, 1998.

[7]Matsumoto, T., Kiuchi, N., and Watanabe, A. Light weight graphite fabric for satellite rflectors. In *Journes Internationales de Nice sur les Antennes – International Symposium on Antennas* (November 2002), vol. 2, Journes Internationales de Nice sur les Antennes, pp. 57–60.

[8]Rayleigh, J. W. S. *Theory of Sound*, vol. 1. Dover Publications, New York, 1945.

[9]Robinson, S. A. Simplified spacecraft antenna reflector for stowage in confined envelopes. Publication number: 0534110A1, 31 March 1993. European Patent Application filed by Hughes Aircraft Company.

[10]Romeo, R. C., Meinel, A. B., Meinel, M. P., and Chen, P. C. Ultra-lightweight and hyper-thin rollable primary mirror for space telescopes. In *UV, Optical and IR Space Telescopes and Instruments,Proceedings of SPIE* (2000), J. Breckinridge, Ed., vol. 4013, pp. 634–639.

[11]Skelton, J. Triaxially woven fabrics: Their structure and properties. *Textile Research Journal 41*, 8 (August 1971), 637–647.

[12]Tan, L. T. *Thin-Walled Elastically Foldable Reflector Structures.* PhD thesis, Department of Engineering, University of Cambridge, Cambridge, CB2 1PZ, UK, December 2002.

[13]Tan, L. T., and Pellegrino, S. Stiffness design for spring back reflectors. In *43rd AIAA/ASME/ASCE/AHS/ASC Structures, Structural Dynamics and Materials Conference* (Denver Colorado, 22-25 April 2002). AIAA 2002-1498.

[14]Tan, L. T., and Pellegrino, S. Optimization of stiffening system for spring-back reflectors. In *EUROMECH 442 International Colloquium on Computer-Aided Optimization of Mechanical Systems* (Erlangen, Germany, 23-27 February 2003).

[15]Tan, L. T., and Pellegrino, S. Ultra thin deployable reflector antennas. In *45rd AIAA/ASME/ASCE/AHS/ASC Structures, Structural Dynamics and Materials Conference* (Palm Springs, California, 19-21 April 2004). AIAA 2004-1730.

[16]Tan, L. T., and Pellegrino, S. Stiffening method for thin shell deployable reflectors: Part 1, approach. Submitted to AIAA Journal, 2005.

[17]Watanabe, A., Tadokoro, H., and Arai, Y. Tensile properties of twf reinforced cf/ep single ply composites. In *Materials and Process Affordability, Keys to the Future* (June 1998), H. S. Kliger, Ed., vol. 43 of *43rd International SAMPE Symposium and Exhibition*, Society of Advancement of Material and Process Engineering (SAMPE), SAMPE, pp. 1874–1882.

[18]Yee, J. C. H., O, S., and Pellegrino, S. Carbon fibre reinforced plastic tape springs. In *45th AIAA/ASME/ASCE/AHS/ASC Structures, Structural Dynamics and Materials Conference* (Palm Springs, 19-22 April 2004). AIAA 2004-1819.